

PAPER • OPEN ACCESS

## Fluid flow in steady and oscillatory lid-driven square cavities

To cite this article: J Zhu *et al* 2017 *IOP Conf. Ser.: Mater. Sci. Eng.* **276** 012015

View the [article online](#) for updates and enhancements.

### Related content

- [Applications of the CE/SE Scheme to Incompressible Viscous Flows in Two-Sided Lid-Driven Square Cavities](#)  
Yang Duo-Xing and Zhang De-Liang
- [The effect of different aspect ratio and bottom heat flux towards contaminant removal using numerical analysis](#)  
M N A Saadun, C S Nor Azwadi, Z A A Malek et al.
- [The onset of centrifugal instability in an open cavity flow](#)  
Christelle L Douay, François Lusseyran and Luc R Pastur



IES Ltd. develops the Virtual Environment (VE), the world-leading building simulation software which enables clients to design innovative buildings while minimising the impact on the environment. The VE is the only tool which allows designers to simulate the full performance of their design.

The successful candidate will join a team developing state-of-the art code for advanced building and district physics simulation. The team employs mathematical modelling techniques to analyse heat transfer mechanisms, air conditioning, renewable energy systems, natural ventilation, lighting, thermal comfort, energy consumption, carbon emissions and climate, and assess building performance against regulatory codes and standards in different countries.

[careers@iesve.com](mailto:careers@iesve.com)

# Fluid flow in steady and oscillatory lid-driven square cavities

<sup>a</sup>J Zhu, <sup>a</sup>L E Holmedal, <sup>a</sup>D Myrhaug, <sup>a</sup>H Wang

<sup>a</sup>*Dept. of Marine Technology, Norwegian University of Science and Technology, Trondheim, Norway*

E-mail: jianxun.zhu@ntnu.no

**Abstract.** This paper presents numerical simulations of steady and oscillatory lid-driven cavity flow at different Reynolds numbers with a fixed aspect ratio of 1:1. A projection method (P2 pressure correction method) is applied to solve the incompressible Navier-Stokes equations. The code is validated by comparison with published works of steady lid-driven flow at  $Re = 100, 400$  and  $1000$ . Oscillatory lid-driven cavity flow at different Reynolds numbers ( $100, 400$  and  $1000$ ) at a fixed oscillation frequency has been investigated. It is observed that the oscillatory lid-driven cavity flow is substantially affected by the Reynolds number.

## 1. Introduction

Steady lid-driven cavity flow is one important benchmark for Navier-Stokes solvers due to its simple geometry and can also serve as a simplified model for industrial applications like e.g. wave-induced flow in sandpits (see e.g. [1]). Flow phenomena such as corner vortices and longitudinal vortices exist within the cavity. Flow structures in the cavity vary significantly at different Reynolds numbers  $Re = Uh/\nu$  and aspect ratios  $D = h/l$  (where  $\nu$ ,  $U$ ,  $h$  and  $l$  are the kinematic viscosity of the fluid, the steady lid motion velocity, the depth and width of the cavity, respectively). Flow in a square cavity was investigated extensively by [2]. The predictions, limited up to  $Re = 400$ , show that there are three vortices existing in the cavity (one primary vortex occupying the central core and two other relatively small vortices located at the bottom corners of the cavity). Steady square lid-driven cavity flow at  $Re \leq 10000$  was presented by [3] and [4]. The primary vortex and two corner vortices grow in strength as the Reynolds number increases while an upper left wall vortex is observed when the Reynolds number increases to 3200.

A few studies have been carried out for flow in a square cavity driven by an oscillating wall. The vortex dynamics have been investigated by [5] at different Reynolds numbers and Stokes numbers (here, the Stokes number is  $St = \omega A^2/\nu$ , where  $\omega$  and  $A$  are the frequency and amplitude of the lid motion) for equal values ( $Re = St$ ) ranging from 0 to 600. It is observed that one counter-rotating vortex pair and two corner vortices occur within the cavity during one cycle. Similar results have also been presented by [6], [7] and [8].

In the present paper, the steady lid-driven cavity flow at different Reynolds numbers has been investigated and compared with corresponding results obtained from [4]. Simulations of the oscillatory lid-driven cavity flow at a fixed oscillation frequency have been conducted at different Reynolds numbers. The results show good agreement with the previous data presented



by [8]. This approach facilitates a detailed study of the oscillatory lid-driven cavity flow covering a wide range of physical parameters in terms of Stokes numbers and Reynolds numbers.

## 2. Problem formation

A definition sketch of the flow in a square lid-driven cavity is shown in Figure. 1. The flow is considered to be incompressible and homogeneous. The continuity equation and Navier-Stokes equations are given as:

$$\nabla \cdot \vec{U} = 0 \quad (1)$$

$$\frac{\partial \vec{U}}{\partial t} + \vec{U} \cdot \nabla \vec{U} = -\frac{1}{\rho} \nabla p + \nu \Delta \vec{U} \quad (2)$$

where  $\vec{U}$  is the velocity vector with the horizontal velocity component  $u$  and vertical component  $w$ ;  $Re = U_{lid}h/\nu$  for steady lid-driven cavity flow and  $Re = U_{max}h/\nu$  for oscillatory lid-driven cavity flow (where  $U_{lid}$  is the steady velocity and  $U_{max}$  is the velocity amplitude, respectively). Moreover, the velocity presented in this paper is scaled by  $U_{lid}$  and  $U_{max}$  for the steady and the oscillatory lid-driven flow, respectively. No-slip velocity and Neumann pressure conditions are imposed on all the walls.

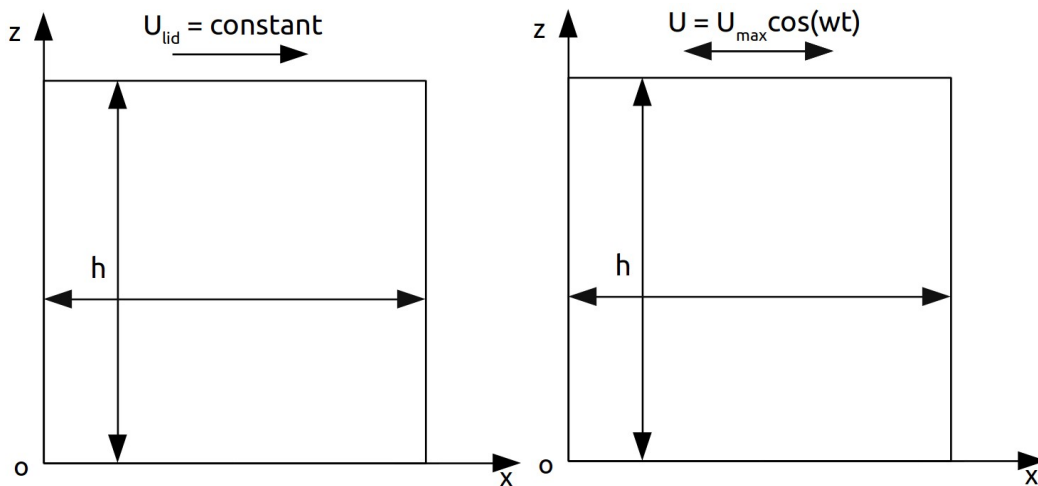


**Figure 1.** Schematic of the steady and oscillatory lid-driven cavity flow.

## 3. Numerical method

Equations (1) and (2) are discretized by second order central differences in space with a staggered grid arrangement. The impulse equations have been integrated in time using a semi-implicit second order scheme in conjunction with a projection method, where Adams-Bashforth and Crank-Nicolson are applied to the convective terms and diffusive terms, respectively.

A P2 projection method has been applied in a standard manner to solve the Navier-Stokes equations. Here an intermediate velocity field (which does not satisfy the continuity equation) is obtained by using the pressure gradient from the last time step (P2 method). A Poisson equation for the pressure is solved in such a way that the resulting pressure gradients are applied to correct the intermediate velocity field such that the resulting velocity satisfies the continuity equation.

## 4. Results of test cases and examples

### 4.1. Grid convergence test

The grid convergence test is carried out by using the predictions of the steady lid-driven flow in a square cavity at  $Re = 100, 400$  and  $1000$ . Five different uniform grid resolutions have

been applied for each Reynolds number. The minimum values of the velocities  $u(0.5, z/h)$  and  $w(x/h, 0.5)$  and the maximum values of  $w(x/h, 0.5)$  are shown in Table 1. At  $Re = 100$ , these values obtained from  $64 \times 64$  grid cells deviate less than 0.1% from those obtained from  $48 \times 48$  grid cells. As the Reynolds number increases to 400, the deviation between the values from  $96 \times 96$  and  $128 \times 128$  grid cells is less than 0.1% while for  $Re = 1000$ , this deviation is obtained between  $128 \times 128$  and  $160 \times 160$  grid cells.

**Table 1.** Results of cases with different grid resolutions

Test Cases	Velocity at the central line		
	$\min_z u(0, z/h)$	$\min_x w(0, x/h)$	$\max_x w(0, x/h)$
32	-0.2072	-0.2461	0.1734
48	-0.2099	-0.2488	0.1757
64	-0.2111	-0.2499	0.1765
96 <sup>a</sup>	-0.2117	-0.2506	0.1771
128	-0.2120	-0.2508	0.1773
Re = 100			
48	-0.3118	-0.4352	0.0.2871
64	-0.3179	-0.4417	0.2933
96	-0.3225	-0.4472	0.2976
128 <sup>a</sup>	-0.3242	-0.4493	0.2991
160	-0.3250	-0.4498	0.2998
Re = 400			
64	-0.3634	-0.4970	0.3524
96	-0.3753	-0.5117	0.3636
128	-0.3797	-0.5172	0.3679
160 <sup>a</sup>	-0.3818	-0.5197	0.3699
192	-0.3825	-0.5207	0.3703
Re = 1000			

<sup>a</sup>The case for investigation.

#### 4.2. Two-dimensional steady lid-driven flow in a square cavity

The steady flow predictions with  $Re = 100, 400$  and  $1000$  are presented in this section. Figure 2 depicts the velocity profiles on the center-line of the cavity showing good agreement with the corresponding results obtained from [4]. The slope of the velocity profiles  $u(0.5, z/h)$  and  $w(x/h, 0.5)$  is nearly constant in the core region (i.e. away from the wall) for a Reynolds number of 1000. Moreover, the region with near uniform vorticity grows with increasing Reynolds number as shown in Figure 3. It is demonstrated that the thickness of the boundary layers at the walls decreases as the Reynolds number increases.

Figure 4 shows streamlines for the primary vortex and corner vortices at  $Re = 100, 400$  and  $1000$ . The primary vortex core moves towards the centre of the cavity and increases in strength while the corner vortices grow both in size and strength as the Reynolds number increases. The right corner vortex is smaller and weaker than the left vortex. Moreover, the stream-function and the vorticity contours are in good agreement with the results in [4].

#### 4.3. Two-dimensional oscillatory lid-driven flow in a square cavity

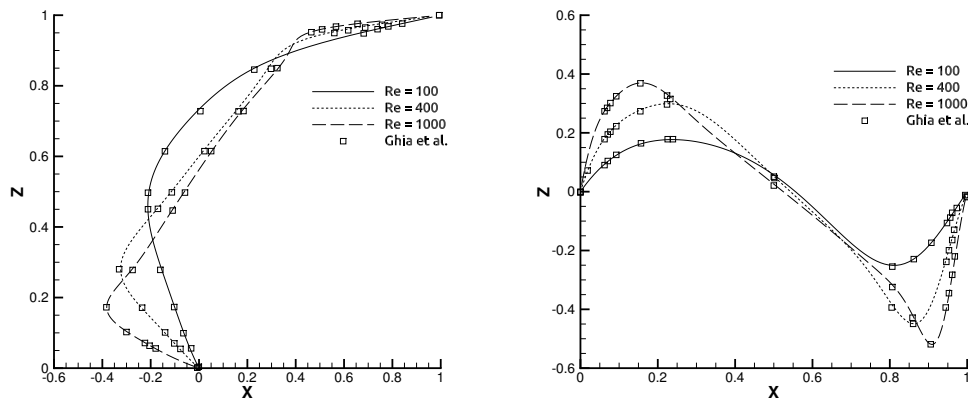
Here results for the periodic solutions on the oscillatory lid-driven cavity flow at  $Re = 100, 400$  and  $1000$  with a fixed oscillation frequency parameter  $\omega' = \pi/3$  (here,  $\omega' = h\omega/U_{max} = h/A$ )

are given. The results are presented for 10 intervals of each oscillation cycle.

The oscillatory lid-driven cavity flow is expected to give a time-periodic flow. The criterion for the flow being fully developed is:

$$\frac{\max|\vec{U}^n(x, z, t + T) - \vec{U}^{n-1}(x, z, t)|}{\max|\vec{U}^n(x, z, t)|} \leq \epsilon \quad (3)$$

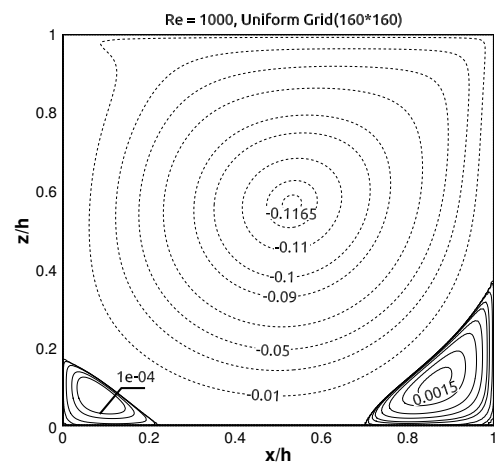
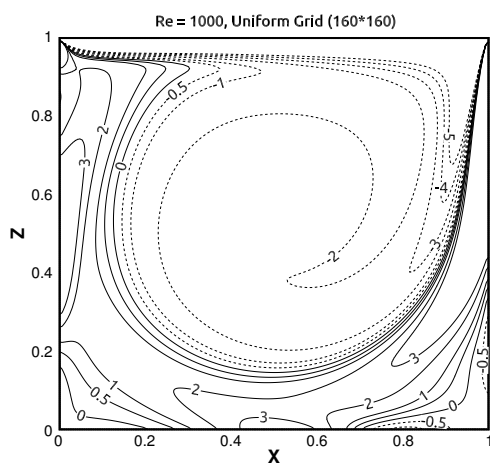
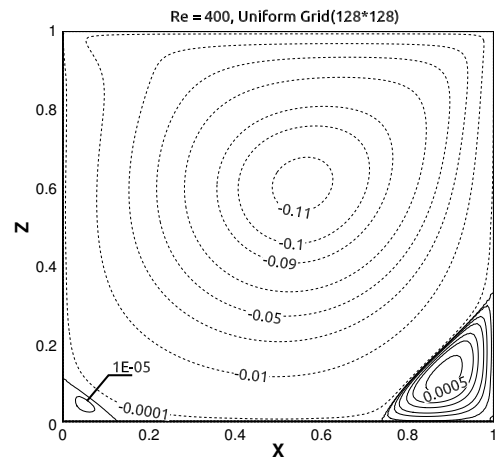
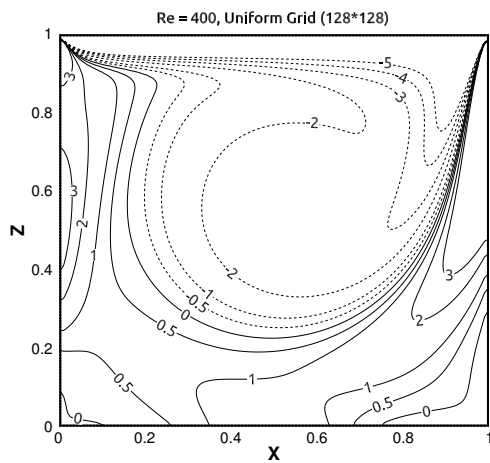
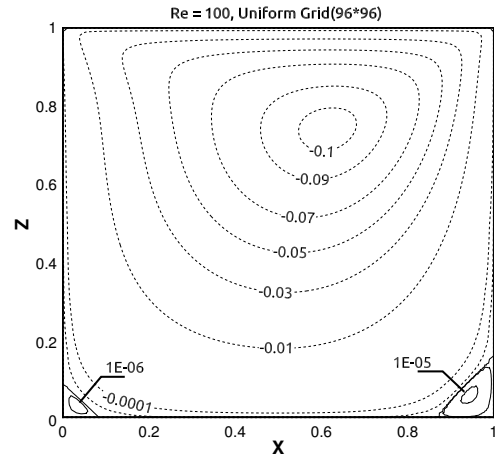
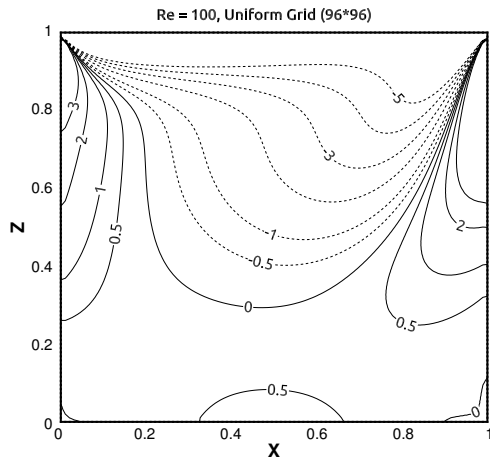
where  $n$  denotes the time step number;  $\epsilon = 1 \times 10^{-6}$  and  $T$  is the period of the lid motion.



**Figure 2.** Comparisons of  $u(0.5, z/h)$  and  $w(x/h, 0.5)$  between predictions of the steady lid-driven cavity flow and reference data from Ghia et al. [4] at various Reynolds numbers

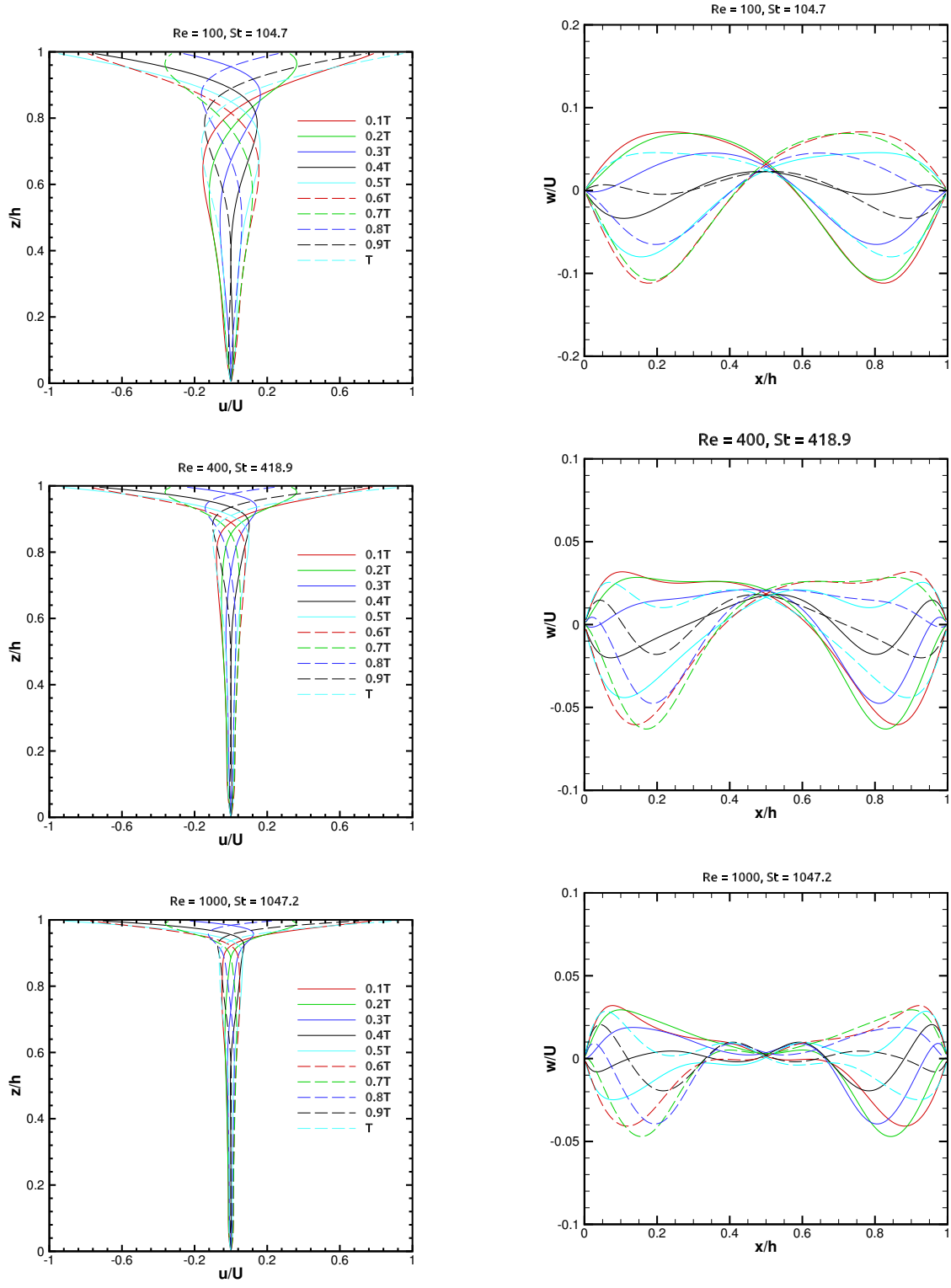
Figures 5 and 6 show the velocity profiles  $u(0.5, z/h)$  and  $w(x/h, 0.5)$ , respectively. It is observed that the velocity profiles at  $t$  and  $t + T/2$  are mirror images of each other. Comparison with the results in Fig. 2 reveals that the velocity profiles for the oscillatory lid-driven cavity flow are more complex than those for the steady lid-driven cavity flow. For instance, the velocity  $u(0.5, z/h)$  at  $t = 0.3T$  changes from a negative value to a positive maximum, and then decreases again to a negative value. Thereafter, it increases gradually to zero as it approaches the bottom wall. In other words, the direction of the velocity changes twice along the center-line indicating that at least one counter-rotating vortex pair emerge in the central region of the cavity. The boundary layer thickness beneath the moving lid decreases as the Reynolds number and consequently the Stokes number increase. This is consistent with laminar boundary layer theory (i.e. Stokes second problem described in [9]); the boundary layer thickness increases as the oscillation period (i.e. Stokes number) increases. Furthermore, the number of local extrema of  $w(x/h, 0.5)$  increases as the Reynolds number increases. This indicates, as shown in Figure. 7 that the number of vortices near the central plane of the cavity increases.

Figure. 7 shows streamlines for different Reynolds numbers at  $t = 0.4T$ . The location and number of vortices within the cavity change for different Reynolds numbers. At  $Re = 100$ , two counter-rotating vortices occur in the cavity (one primary counterclockwise vortex and one small clockwise vortex are formed during the initial phase of the lid motion). As the Reynolds number increases from 100 to 400, an additional counterclockwise vortex appears beneath the clockwise vortex, and the size of the clockwise vortex increases. At  $Re = 1000$ , four vortices appear in the cavity, comprising two counter-rotating vortex pairs. Thus it appears that the flow structures in the cavity become more complex as the Reynolds number increases. The results for  $Re = 100, 400$  and  $1000$  with  $\omega' = \pi/3$  are in good agreement with results obtained by [8].



**Figure 3.** Contours of  $y$ -vorticity for the steady lid-driven cavity flow at different Reynolds numbers

**Figure 4.** Contours of stream-function for the steady lid-driven cavity flow at different Reynolds numbers



**Figure 5.** Profiles of  $u(0.5, z/h)$  for the oscillatory lid-driven cavity flow at different Reynolds numbers with a fixed  $\omega' = \pi/3$

**Figure 6.** Profiles of  $w(x/h, 0.5)$  for the oscillatory lid-driven cavity flow at different Reynolds numbers with a fixed  $\omega' = \pi/3$ . Velocities at different time instants are marked by the same color as in Figure. 5.

## 5. Summary and Conclusions

The flow features in the steady and oscillatory lid-driven cavity have been investigated. It appears that the oscillatory lid-driven flow exhibits more complex fluid dynamical behaviors than the steady lid-driven flow. For the chosen oscillation frequency, the boundary layer thickness at the top lid decreases as the Reynolds number increases. Finally, the number of vortices appearing in the central part of the cavity increases with increasing Reynolds number.

## Acknowledgment

The first author would like to thank the support from the Department of Marine Technology, NTNU and the China Scholarship Council (Grant no. 201506680058).

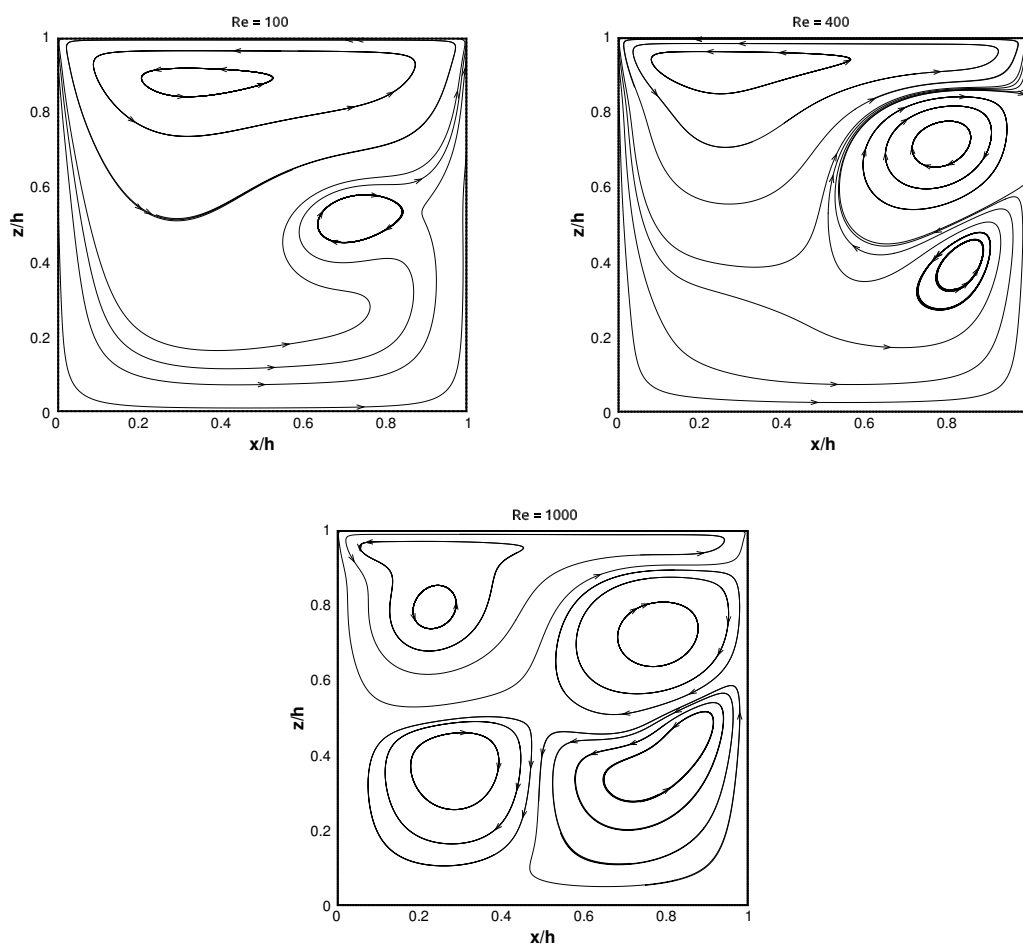


**Figure 7.** Streamline patterns of the oscillatory lid-driven flow with different Reynolds numbers at  $t = 0.4T$ .

## References

- [1] Van Rijn L, Soulsby R, Hoekstra P and Davies A 2005 *SANDPIT, Sand Transport and Morphology of Offshore Mining Pits*.
- [2] Burggraf O R 1966 *J. Fluid Mech.* **24**(1) 113–151
- [3] Benjamin A and Denny V 1979 *J. Comput. Phys.* **33**(3) 340–358
- [4] Ghia U, Ghia K N and Shin C 1982 *J. Comput. Phys.* **48**(3) 387–411



- [5] Duck P 1982 *J. Fluid Mech.* **122** 215–234
- [6] Liu C H 2001 *Int. J. Numer. Methods Fluids* **35(5)** 533–557
- [7] Iwatsu R, Hyun J M and Kuwahara K 1992 *J. Fluids Eng.* **114(2)**
- [8] Mendu S S and Das P 2013 *Eur. J. Mech. B. Fluids* **39** 59–70
- [9] Hermann S *et al.* 1979 *McGarw-Hill Book Company* 135–149